Absorption and photoluminescence spectroscopy of rubrene single crystals

Pavel Irkhin,[1] Aleksandr Ryasnyanskiy,[1] Marlus Koehler,[2] and Ivan Biaggio[1]
[1]*Department of Physics, Lehigh University, Bethlehem, Pennsylvania 18015, USA*
[2]*Departamento de Fisica, Universidade Federal do Paraná, Curitiba, Brazil*
(Received 6 June 2012; revised manuscript received 6 August 2012; published 27 August 2012)

We report the intrinsic absorption and photoluminescence spectra of rubrene single crystals, deriving them from a series of experiments performed at different excitation wavelengths and in different experimental geometries. We describe the absorption spectra for all three light polarizations in the crystal, and discuss how anisotropic wavelength-dependent absorption and emission affect the characteristics of observed photoluminescence spectra. We identify vibronic progressions both in absorption and emission and discuss their parameters and the main vibrational modes that are responsible for them. We propose that the most commonly measured absorption and emission in rubrene, the one with light polarization perpendicular to the c axis of the crystal, is caused by vibronic-induced depolarization of the c-polarized electronic transition between the highest occupied molecular orbital (HOMO) and the lowest unoccupied molecular orbital (LUMO).

DOI: 10.1103/PhysRevB.86.085143 PACS number(s): 81.05.Fb, 78.40.Me, 71.35.−y, 78.55.Kz

I. INTRODUCTION

The optical absorption and photoluminescence spectra of organic molecular crystals depend on the optical properties of the constituent molecules, on the geometrical arrangement of the molecules in the crystal matrix, and on intermolecular interactions. The rubrene single crystal has a large optical anisotropy that has a strong influence on the absorption and luminescence spectra that are observed under different experimental conditions. Although transport properties of rubrene single crystals have been extensively studied, considerably fewer studies have explored their optical properties, in particular the characteristics of the observed photoluminescence.

Among several organic materials that have been used as organic semiconductors, e.g., in organic field-effect transistors,[1–3] photovoltaic cells,[4] or light emitting diodes,[5] rubrene single crystals are of particular interest because of several compelling properties, including one of the highest room-temperature charge carrier mobilities ever observed in an organic material ($\sim$10–40 $\mathrm{cm^2V^{-1}s^{-1}}$ for holes in field-effect transistors[1,6–9]) and a high photoconductivity.[10–12] The high hole mobility values in rubrene crystals are found along the crystallographic direction characterized by a herringbone packing with an efficient π-orbital overlap.

In this work, we obtain a complete set of absorption and emission spectra for the rubrene single crystal, describe location and relative strength of the various photoluminescence bands that are intrinsic to rubrene single crystals, and we discuss the relation of these spectra with each other, with the experimental geometry, and with previous results in the literature.

The properties of the rubrene molecule and how it is oriented in the crystal introduce a peculiar sensitivity of the detected photoluminescence spectrum from the experimental conditions, such as which facet of a crystal is illuminated, the surface quality of the crystal facet, and the wavelength used for photoexcitation. Because of this, photoluminescence spectra of rubrene single crystals reported up to now (see, e.g., Refs. 13–22) partially contradict each other both in the actual data as well as in the interpretations proposed by the various authors.

In the following, we present a detailed review of the way in which different experimental conditions in rubrene give rise to large variations in the detected photoluminescence spectra. We then extract the intrinsic emission spectra taking into account the anisotropic absorption of orthorhombic rubrene and the excitation/detection conditions, identifying the underlying emission bands and their energies.

II. RUBRENE MOLECULE AND RUBRENE CRYSTAL STRUCTURE

In general, absorption and photoluminescence (PL) spectra of organic crystals have a molecular exciton signature that is strongly influenced by the optical properties of the individual molecules. Below, we first review optical excitation and emission properties of the rubrene molecule.

Rubrene (5,6,11,12-tetraphenylnaphthacene) belongs to the group of polycyclic aromatic hydrocarbons and consists of four benzene rings (a molecular backbone structurally equal to tetracene) and four substituted phenyl groups attached to the two internal rings. The rubrene molecule as it is found in orthorhombic rubrene single crystals[23] is centrosymmetric, with a symmetry corresponding to the point group $2/m$, or C_{2h}, and a twofold axis of rotation (M axis) along the short backbone. This molecular structure and the directions of the L, N, and M axes are shown in Fig. 1(a). We note that this structure differs in chirality as well as in the angles between the tetracene backbone and the phenyl side groups from the minimum-energy configuration of the rubrene molecule as can be obtained in quantum-chemical calculations.[24,25]

The molecular symmetry C_{2h} allows one to categorize the symmetry of all its states by the four irreducible representations A_g, A_u, B_g, B_u, where A/B refer to states symmetric/antisymmetric with respect to the rotation by 180° (C_2), while the subscripts u/g refer to odd/even parity with respect to the inversion operation. The highest occupied molecular orbital (HOMO) and the ground state of the molecule belong to the totally symmetric representation A_g. A dipole allowed transition can occur to excited states that belong to either the A_u or B_u representations. The A_u state corresponds to the

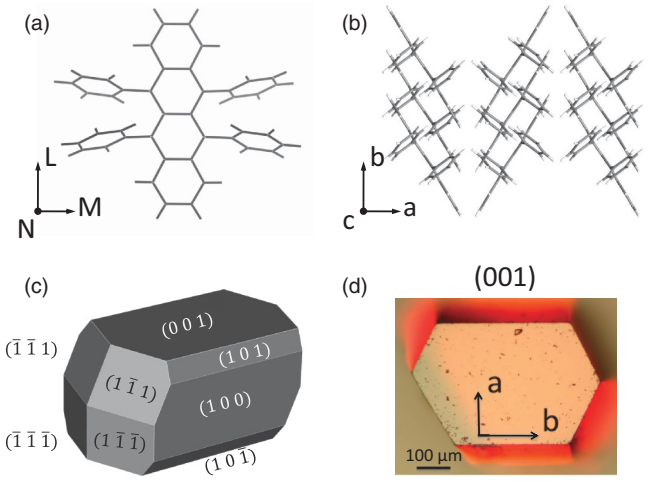

FIG. 1. (Color online) (a) Rubrene molecule; (b) rubrene crystal structure in the ab plane; (c) simulated (Ref. 27) habit of a rubrene single crystal; (d) image of a micrometer-sized stubby rubrene single crystal.

lowest unoccupied molecular orbital (LUMO), while the B_u state is the next higher state. The (L,N,M) components of the dipole operator in the C_{2h} point group have symmetries (B_u,B_u,A_u). HOMO-LUMO transitions ($A_g \leftrightarrow A_u$) are only dipole allowed for a dipole operator of symmetry A_u, because $A_g \otimes A_u \otimes A_u = A_g$. They therefore occur for light polarized along the M axis of the molecule [Fig. 1(a)]. On the other hand, transitions to and from the higher B_u state require a dipole operator with symmetry B_u (because $A_g \otimes B_u \otimes B_u = A_g$), and are therefore associated with light polarized along the L or N axes of the molecule. Transitions between the excited states (symmetry A_u and B_u) are not dipole allowed in this centrosymmetric molecule.

Vapor transport grown rubrene crystals are orthorhombic,[23] with D_{2h}^{18} (or mmm) point group and four molecules per unit cell. In this work, we define the crystallographic axes in the space group $Acam$, in which the lattice constants are $a = 14.4$ Å, $b = 7.18$ Å, and $c = 26.9$ Å instead of $Cmca$, as used in Ref. 23, where a (instead of c) corresponds to the long axis. The reason for this choice is that it is consistent with the labeling of the axes used in several charge transport experiments.[7,10]

Figure 1(b) shows the molecular stacking along the mirror plane of the crystal (ab plane). The L and N axes of the molecules are parallel to the ab plane of the crystal, while the M axes are all parallel to the c direction. When viewed along the normal to the surface, the boundaries of the growth facets parallel to the $\{001\}$ planes form an angle of 63.5 degrees to the b axis, while the boundaries or growth facets parallel to the $\{100\}$ planes form an angle of 75 degrees to the b axis[26] [Fig. 1(c)].

The most common shapes among as-grown rubrene crystals are platelets with extended c surfaces and crystals elongated in the b direction but with small thickness along the c direction. Crystal growth also delivers some high-quality stubby crystals with more equilibrated dimensions (up to $\sim$500 μm) in the three spatial directions. Such crystals exhibit various $\{ijk\}$ surfaces with indices between 0 and 2 [Figs. 1(c)–1(d)]. The analysis of the crystal habit reveals characteristic geometries for the confining surfaces, which offer an unambiguous identification of the orientation of each surface. We observed that the PL properties of such crystals are very stable and do not change even over several years.

III. EXPERIMENT

A. Optical absorption

As discussed in the previous section, the dipole matrix element for the lowest-energy electronic transition from the ground state of the rubrene molecule has only one component, corresponding to the molecular M direction. This characteristic, coupled with the fact that all molecules in orthorhombic rubrene have their M axes parallel to each other, creates a very large absorption and emission anisotropy in rubrene. The strong anisotropic absorption has an extremely large influence on the photoluminescence spectra that can be obtained from rubrene single crystals under different illumination and detection geometries. Before presenting our PL results in the next section, it is therefore necessary to first review and accurately determine the absorption spectra of rubrene for light polarized parallel to the three crystallographic axes.

Since the strongest low-energy transition in the rubrene molecule is M polarized, and since the M axis of all molecules in rubrene is parallel to the c axis of the crystal, we first discuss the absorption spectrum of rubrene for light polarized along the c axis. As-grown crystalline thin platelets have large surfaces that are normal to the c axis. In order to determine the c-polarized absorption spectrum, we measured the transmission of thin rubrene platelets at oblique incidence for light polarized in the plane of incidence. The crystals studied were observed under the microscope to make sure that all surfaces were unblemished. Both direct microscopic observation with a spatial resolution of 0.4 μm and interferometry were used to determine the thickness of the crystals, obtaining values between 0.8 and 5.0 μm for the samples studied. Polarized white light was then focused onto the crystal with a 10× objective (Rayleigh range was always much larger than sample thickness), and the change in its spectrum after passing the crystal was measured with an Ocean Optics USB4000 fiber-coupled spectrometer by capturing the light with a second objective and focusing it into a multimode fiber of 100 μm diameter. We obtained calibrated absolute values for the sample transmission at each wavelength by measuring and correcting any polarization dependence in the reflectivity and transmission of the optical components used in the experiment. Several transmission spectra were collected starting at normal incidence and then for different rotations of the crystal around its a-axis. Angle-dependent reflection losses were both calculated from the refractive indices in the spectral range of interest ($n_a \approx 1.7$, $n_b \approx 1.9$, and $n_c \approx 2.0$[26,28]) and measured experimentally. We used interferometry to confirm the refractive index values and to confirm that index dispersion did not affect our evaluation of the absorption spectra. Finally, the absorption of the crystal for different incident angles was calculated taking into account the reflection losses and the incidence-angle dependent optical path length in the crystal. Figure 2(a) shows absorbance spectra of a 2.7 μm thick rubrene

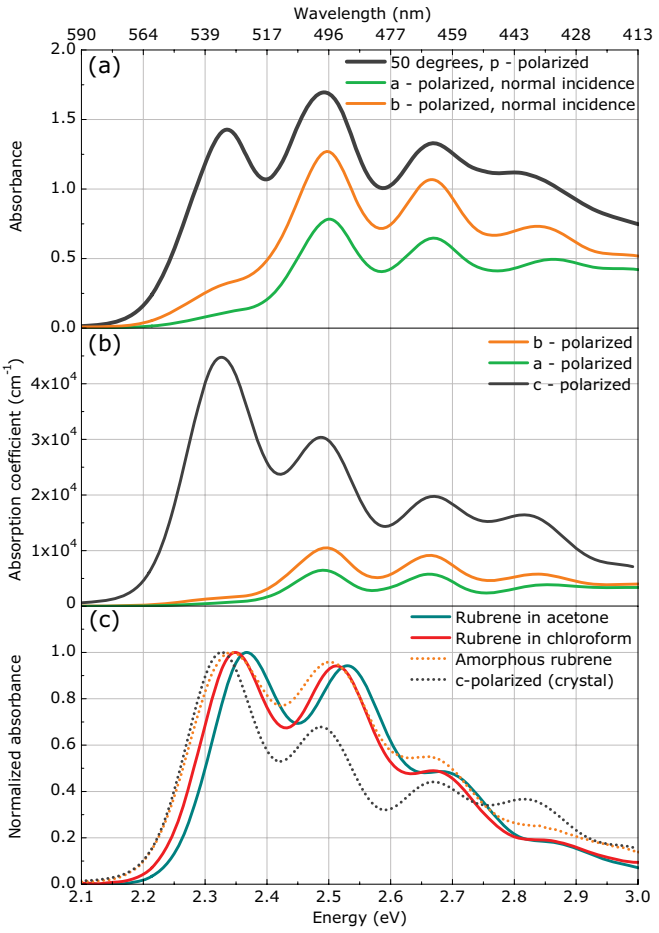

FIG. 2. (Color online) (a) Absorbance spectra of a thin (2.7 μm) rubrene crystal at normal and oblique angles of incidence on the *ab* plane; (b) absorption coefficients of rubrene for light polarized along the main crystal axes derived from multiple experiments; (c) normalized absorbance spectra of rubrene in solutions, amorphous solid, and normalized *c*-polarized absorbance of a rubrene single crystal.

crystal at normal and oblique angles of incidence. At moderate deviations from normal incidence, one immediately observes the emergence of a strong absorption band near 2.32 eV [Fig. 2(a)].

The absorption constant for light polarized in the plane of incidence as a function of the angle θ between the surface normal and the wave vector of the light inside the crystal is

$$\alpha(\theta) = \alpha_{a,b}\cos^2\theta + \alpha_c \sin^2\theta, \qquad (1)$$

where $\alpha_a, \alpha_b, \alpha_c$ are the absorption constants for light polarized along the three crystallographic axes, and in the above equation one must use either α_a or α_b depending on the experimental geometry. By calculating θ from the external angle using Snell's law and comparing the normal incidence spectra for α_a and α_b to the oblique incidence spectra for various values of θ between 10 and 50 degrees in several rubrene crystals, we extracted the full *c*-polarized absorption spectrum up to an energy of 3.0 eV. This spectrum is shown in Fig. 2(b). The *c*-polarized absorption spectrum is dominated by a very strong band at 2.32 eV, followed by less intense bands at 2.49, 2.66, 2.83, and 3.00 eV, separated by 0.17 eV.

For comparison, Fig. 2(c) shows the absorption spectrum of rubrene dissolved in different solvents, and also of an amorphous molecular assembly of rubrene obtained by melting rubrene in an enclosure protected from atmospheric influences (e.g., oxidation). In all the spectra of Fig. 2(c), the absorbance is caused by a rotationally averaged molecular orientation and is therefore dominated by the same transition dipole moment along the molecular *M* axis that determines the *c*-polarized absorption spectrum in the crystal. The strongest absorption band for *c*-polarized light, observed at a photon energy of 2.32 eV in the crystal, is clearly reflected in the spectra of Fig. 2(c).

The absorption constant for light polarized along the *a* and *b* axes of the crystal was obtained from measurements taken at normal incidence. For *a*- or *b*-polarized light, the absorption spectra show a relatively strong band at 2.49 eV, followed by weaker bands at energy intervals of about 0.17 eV. The main features of these spectra agree with earlier reports in the literature.[10,14,22] The *a*- and *b*-polarized spectra also show a small shoulder near 2.32 eV, the energy of the strongest absorption peak visible in the *c*-polarized spectrum. This shoulder becomes more prominent whenever the light used to measure the absorption has a component that is *c* polarized—as when the absorption is measured through more tightly focused beams, or when the incidence angle is not perfectly perpendicular to the *ab* facet of the crystal, which causes a "leakage" of the strong *c*-polarized absorption. This raises the question if this band at 2.32 eV that is seen in *a*- or *b*-polarized spectra may be solely due to this leakage effect. It is certainly possible for *a*- or *b*-polarized measurements to overstate the size of this band. We have seen that the strength of this band can be minimized by measuring absorption using unfocused light, carefully aligning for normal incidence, and using crystals with higher surface quality. But can the whole band be an experimental artifact? From our fitting of the *b*-polarized absorption spectrum [Fig. 3(b), described in the next paragraph), we calculate an $\alpha_b = 400$ cm^{-1} at 2.32 eV that is exclusively due to the tail of the higher-energy bands, while the observed *b*-polarized absorption in our raw spectrum is 1.5×10^3 cm^{-1}. The value of α_c at the same photon energy is 4.5×10^4 cm^{-1}. From Eq. (1) one would need a deviation from normal incidence of the order of only 10 degrees (external angle) to obtain the observed (1500 cm^{-1}) *b*-polarized absorption band at 2.32 eV, assuming perfectly planar wave fronts ($\sim$5 degrees for *a* polarized). Some misalignments, crystal imperfections, and/or light wave-front curvature could result in the observed band at 2.32 eV. The absorption spectra for *a*- and *b*-polarized light in Fig. 2(b) have been measured in a way that minimizes (but does not completely remove) the artificial enhancement of the absorption band at 2.32 eV that is caused by this leakage effect. From these observations, combined with additional insights obtained from the PL spectra analysis that we will present below, we conclude that the observed shoulder at 2.32 eV is probably mainly caused by leakage of the *c*-polarized absorption, and should therefore not be considered as part of the intrinsic *a*- or *b*-polarized absorption spectrum of rubrene.

To evaluate the position, amplitude, and width of the absorption bands contributing to the rubrene absorption spectra, we used a model spectrum consisting of a sum of separate bands to fit all absorption spectra between 2.1 and 3.6 eV.

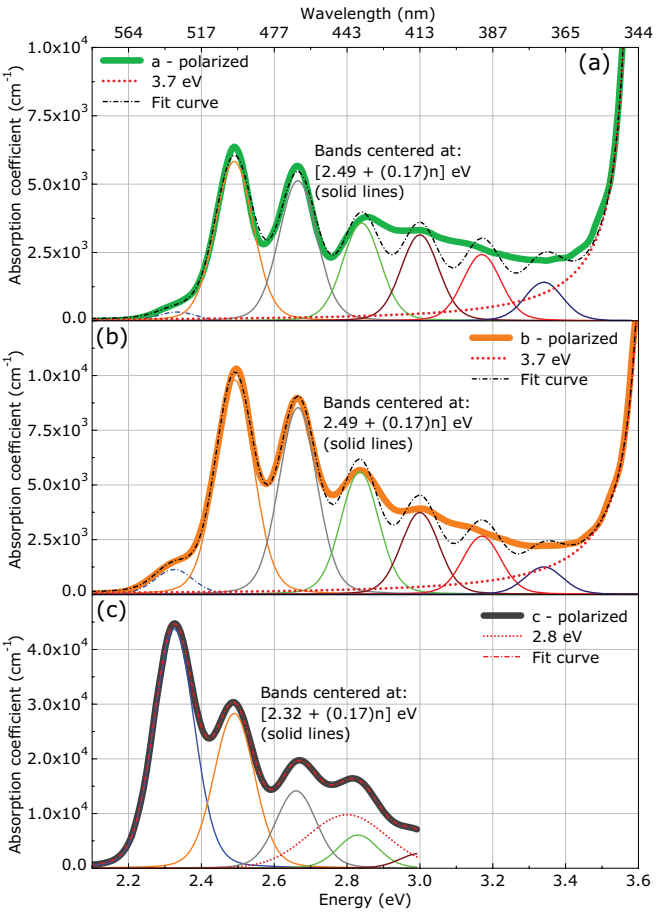

FIG. 3. (Color online) Peak fit of *a*-polarized (a), *b*-polarized (b), and *c*-polarized (c) absorption spectra.

We made a special effort to minimize the number of fitting parameters by using the same identical Voigt profile for every spectral component and by using a sum of these Voigt profiles separated by a constant distance in energy. This corresponds to the simplest possible model for a set of equidistant vibrational levels that determine the vibronic progression. Thus, the only free parameters in the fit are the Lorentzian and Gaussian widths determining the shape of the Voigt profile used for all spectral components, the amplitude of each profile, the distance between them, and the position of the first absorption peak in the progression. In other words, curve fitting of all three absorption spectra in Fig. 3 was done using four parameters for modeling the characteristics of the vibronic progression that all of them share, plus the amplitudes of the individual bands. In addition, to fit the *ab*-polarized spectra we also included the low-energy tail of the higher electronic state close to 3.7 eV.[14,28]

As can be seen in Fig. 3, the experimental absorption spectra can be closely reproduced using a sum of Voigt profiles with full width at half maximum (FWHM) of 0.12 eV and a ratio between Gaussian and Lorentzian widths of 5.6. The first band is at 2.32 eV, and it is followed by a sequence of higher-energy bands, all separated by 0.17 eV. The absorption band at 2.32 eV that we have earlier assigned to an artificial "leakage" is drawn using a dash-dotted line. For the *c*-polarized spectrum [Fig. 3(c)], the fitting function included an additional, noticeably wider band positioned at 2.8 eV. This band appears as a major difference between the absorption of a crystal and that of rubrene molecules in solution or in an amorphous solid, as can be seen in Fig. 2(c). Such a band was also reported in the *c*-polarized absorption spectrum derived from ellipsometry data by Tavazzi *et al.*,[29] where it was dominating the spectrum at around 2.8 eV, and the higher vibronic replicas were not resolved. We observed that the relative strength of this extra band slightly varies between samples of different thickness. The existence of this additional absorption band at 2.8 eV is supported by a theoretical prediction of a quasiparticle band gap of 2.8 eV by Sai *et al.*[28] Finally, we note that our simple model spectrum can reproduce the *c*-polarized spectrum extremely well, with the model function (dash-dotted line) practically indistinguishable from the data. On the other hand, there are deviations between the fitted model function and data in the *ab*-polarized spectra between 2.8 and 3.4 eV that are clearly caused by the fact that we constrained our fitting function to a sum of equally separated vibrational bands with same shape and width. While it would be possible to obtain a better fit by also fitting position and width of the spectral components, such a fit would only increase the number of fitting parameters while not providing any additional information.

B. Photoluminescence

In this section, we review the different photoluminescence (PL) spectra that can be obtained from rubrene crystals under different experimental conditions. We excite the photoluminescence with a linearly polarized CW laser at 2.8 eV (442 nm) or 2.3 eV (532 nm). The laser beam is focused on the sample by a microscope objective, which also collects photoluminescence and images it onto an optical fiber coupled to a spectrometer. A linear polarizer is placed before the fiber to select the polarization of the detected PL. All measurements were done with an Olympus IX81 microscope to ensure a precise orientation of the crystal with respect to the direction and polarization of the excitation beam and for a precise control of crystal surface quality. As we will see later, the latter is very important for spectroscopy done on the *ab* facet, the largest as-grown surface of a rubrene crystal.

The raw PL spectra obtained from *ab* and *bc* facets of rubrene single crystals at two different excitation wavelengths are shown in Fig. 4. Each plot contains four curves, corresponding to the four possible combinations of excitation light and PL polarization. Each curve is labeled with a pair of letters to indicate the crystallographic axis along which the corresponding light polarization is oriented. The first letter gives the polarization of the excitation light; the second letter gives the corresponding orientation of the analyzer in front of the PL detection system.

The vertical scale in the plots in Fig. 4 represents the same PL quantum efficiency for all excitation and emission polarizations, belonging to the same excitation wavelength. One can therefore directly compare the strength of the PL when going from one experimental configuration to the other. To guarantee this we (1) kept the intensity distribution in the excitation spot and the laser power constant, (2) corrected all spectra for a polarization-dependent instrumental response

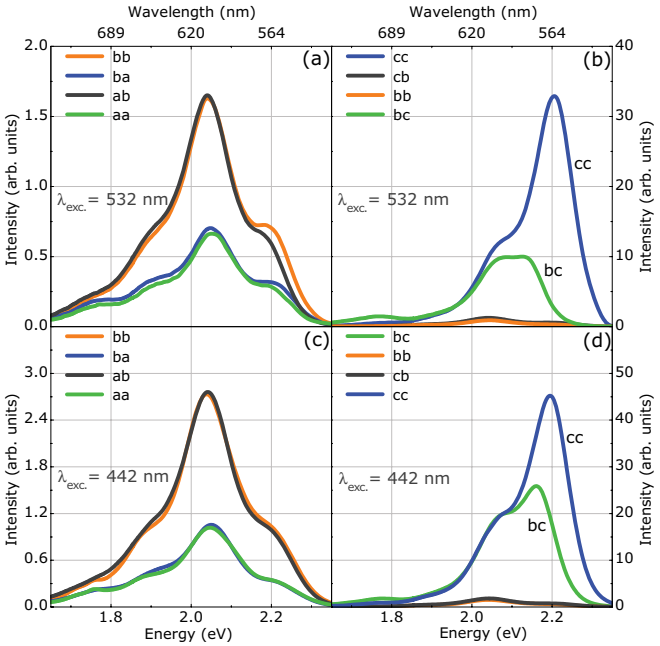

FIG. 4. (Color online) Top: PL spectra measured with 532 nm excitation on *ab* (a) and *bc* (b) facets. Bottom: PL spectra measured with 442 nm excitation on *ab* (c) and *bc* (d) facets. The vertical scale is in the same units for all spectra taken at the same excitation wavelength.

(beam splitter transmittance, spectrometer sensitivity, etc.), and (3) made sure that the PL is collected with equal efficiency for all excitation/detection configurations by keeping the depth of field of the imaging system larger than the absorption length of the material at the excitation wavelength. At 442 nm, the absorption length of rubrene is about 3 μm for *a*-polarized light, 2 μm for *b* polarization, and 0.6 μm for *c* polarization. The corresponding values for 532 nm excitation are 15, 6, and 0.2 μm, respectively. We used a 10× objective with numerical aperture (NA) of 0.3 and a depth of field of 10 μm. In addition to having a large enough depth of field, using such an objective also guarantees that we capture the PL from all photoexcited excitons even in the presence of a 4 μm exciton diffusion length along the *b* axis.[30]

The raw spectra in Fig. 4 have several interesting features. First, we note that in the measurements in Figs. 4(a) and 4(c) the intensity of the PL emission does not depend on the *excitation* light polarization or wavelength, even though the absorption coefficients are different in all cases. The reason for this is that, in a thick crystal, the entire incident light is absorbed in a few micrometers independently of the polarization or wavelengths used, and the created PL is collected with the same efficiency. Then, we note that the *b*-polarized emission spectrum detected from the *bc* facet [Figs. 4(b) and 4(d)] is the same in amplitude and shape as the *b*-polarized emission spectrum detected from the *ab* facet, but it appears very small in Figs. 4(b) and 4(d) because of the large relative strength of the *c*-polarized emission: the peak PL emission is about 20 times larger when detecting *c*-polarized PL [Figs. 4(b) and 4(d)] than when detecting *b*-polarized PL [Figs. 4(a) and 4(c)]. Finally, the most striking differences are observed for *c*-polarized PL: the amplitude of the higher energy peak of the emission spectrum and its position are strongly dependent on the *excitation* polarization and wavelength [Figs. 4(b) and 4(c)]. Some of these observations have been partially reported before.[13,15–21] In particular, the shift of the PL band maximum from 2.19 to 2.16 eV when changing the polarization of the excitation light has been previously reported in Ref. 18, but without discussing it. A large variability of the observed PL spectra in the references above has led to a number of inconsistent interpretations. We will discuss some of the erroneous interpretations in the next section, together with a review of experimental artifacts that can modify the PL spectrum.

All the spectra in Fig. 4, and also all those reported in the literature to date, can be reconciled by taking into account the strong absorption anisotropy of rubrene single crystals. In the following, we show that all spectra originate from three intrinsic polarized emission spectra, which are then deformed by the choices of excitation and detection conditions. The most important effect that needs to be considered is the strong absorption of the intrinsic PL by the material itself, in particular for higher emission energies and for *c*-polarized emission, where the rubrene absorption is strongest. Using the absorption spectra that we presented in Fig. 3, we can calculate quantitatively the effects of absorption and reabsorption (also known as self-absorption) on the PL emission spectra. They depend on the amount of overlap between photoluminescence and absorption spectra, and on the depth at which excitation occurs when compared to the absorption length of the emitted PL.

The amount of PL power detected in a direction normal to the surface is proportional to the amount of excitation light deposited at a given depth inside the crystal, multiplied by the amount of PL light that can reach the surface of the crystal, and integrated over all depths. Hence, the detected spectrum $PL_d(\omega)$ is related to the intrinsic spectrum $PL(\omega)$ by

$$PL_d(\omega) = PL(\omega)\alpha \int_0^\infty e^{-\alpha x} e^{-\alpha(\omega)x} dx = PL(\omega)\frac{\alpha}{\alpha + \alpha(\omega)}, \quad (2)$$

where α is the absorption coefficient for the excitation light and $\alpha(\omega)$ is the absorption coefficient for the emitted PL. The intrinsic spectrum can be recovered from the measured one by multiplying it with $[1 + \alpha(\omega)/\alpha]$. Here, it is understood that one must use the absorption coefficient values for the given light polarization, as given by the appropriate absorption curve in Fig. 3. Figure 5 compares the change of the experimental *c*-polarized PL emission spectrum for different excitation polarizations with the evolution of the same spectrum as can be modeled using Eq. (2). It also shows a similar deformation of the emission spectrum [Fig. 3(c)] when measuring rubrene solutions with different concentrations. The real spectrum is measured at the lowest concentrations, while at higher concentrations an artificial redshift of the emission peak occurs.

For the data in Fig. 5 we chose 532 nm (2.33 eV) for excitation, because at this photon energy the contrast between *b*- and *c*-polarized absorption constants is the largest (Fig. 3). Under these excitation conditions, the distortion of the PL spectrum is expected to be minimal for *c*-polarized excitation

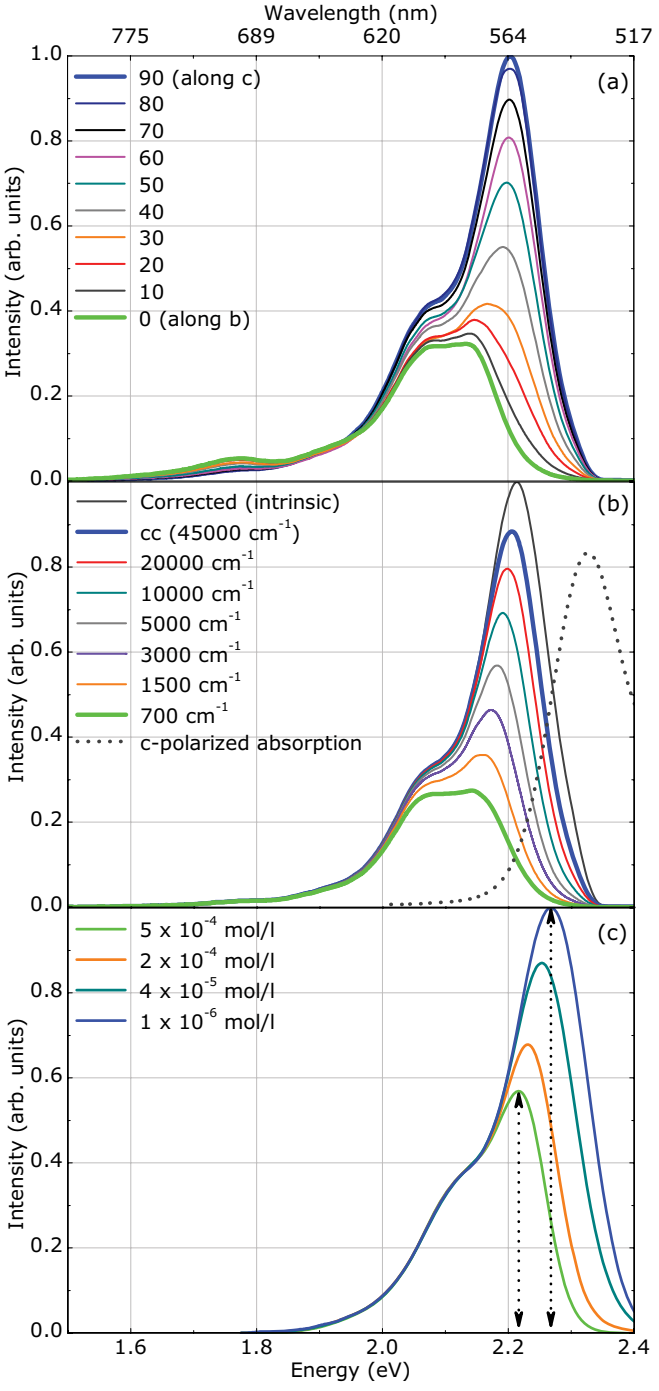

FIG. 5. (Color online) (a) Experimental PL spectra measured on *bc* facet of a rubrene single crystal with 532 nm excitation light polarized at various angles from the *b* axis. (b) Modeling of reabsorption effect on the appearance of the PL spectra. (c) Effect of reabsorption on PL spectrum of rubrene in solution at various concentrations.

(PL originates close to surface), and maximal for pure *b*-polarized excitation (PL originates deeper inside the crystal). This can be clearly seen in Fig. 5(a), where the spectrum excited by the *b*-polarized light is strongly attenuated in the higher-energy parts. The intrinsic PL emission spectrum can be obtained by applying Eq. (2) to the data obtained with *c*-polarized excitation. From this, it is then possible to predict the behavior when rotating the excitation polarization towards the *b* axis. This is done in Fig. 5(b), which shows the intrinsic spectrum as well as the experimental spectrum obtained with *c*-polarized excitation and the spectra predicted for all other intermediate excitation polarizations. The evolution of the spectra matches the observed experimental behavior very well. However, the exact value of the absorption coefficient for *b*-polarized excitation light is very important to match the experimental results. Here we find that the experimental results are reproduced by assuming that the absorption coefficient for the excitation light at 532 nm (2.33 eV) is less than what was experimentally determined in Fig. 2(b). We find that the *b*-polarized absorption coefficient must be $\alpha_b = 700\ \mathrm{cm}^{-1}$ instead of $1500\ \mathrm{cm}^{-1}$ to fit the PL emission data. This confirms that the measured *b*-polarized absorption spectrum is affected by leakage of the strong *c*-polarized absorption (see discussion above). In fact the absorption coefficient $\alpha_b = 700\ \mathrm{cm}^{-1}$ at 2.33 eV that is needed to reproduce the effect of the excitation polarization on the PL spectrum is very close to the value of $\alpha_b = 400\ \mathrm{cm}^{-1}$ that can be assigned to the tail of higher-energy bands. The small difference between these two values could be explained by an additional temperature-induced broadening

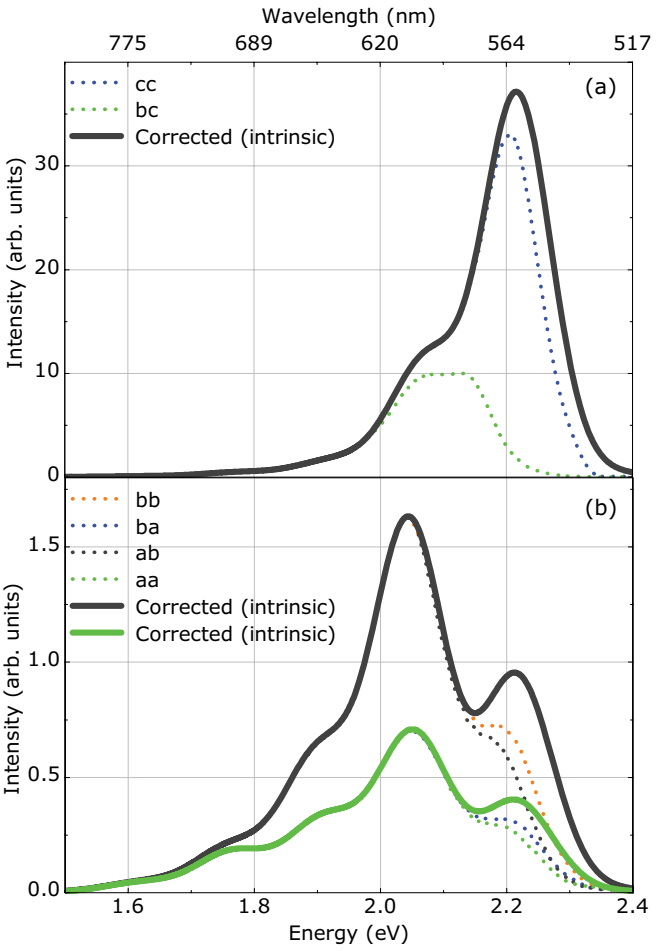

FIG. 6. (Color online) PL spectra for *c*-polarized emission (a) and for *ab*-polarized emission (b) of a rubrene single crystal with corresponding spectra corrected for reabsorption. The spectra were taken from *bc* (a) and *ab* (b) facets.

of the absorption bands, which is present under CW laser excitation.

The procedure outlined above to analyze the PL emission spectra can be used to obtain the intrinsic PL emission spectra from the experimental data in Fig. 4. The results are shown in Fig. 6. The intrinsic spectra in this figure are derived from multiple experiments like those shown in Fig. 4 using Eq. (2) and the absorption spectra in Fig. 3. These intrinsic spectra do not depend on the excitation/detection geometry or on the wavelength or the polarization of the excitation. We confirmed this by using several wavelengths for the excitation from the UV to the visible spectral range (325, 405, 442, and 532 nm) and also by using a 1 picosecond pulsed laser at 488 nm.

Following the same procedure used when analyzing the absorption spectrum, we modeled the intrinsic PL emission spectra presented in Fig. 6. Again, we took care of minimizing the number of fitting parameters, choosing a model function that uses a sum of identical Voigt profiles separated by the same energetic distance. Five Voigt profiles (FWHM is 0.13 eV, ratio between Gaussian and Lorentzian widths is 11) separated by 0.147 eV closely reproduce the intrinsic c-polarized photoluminescence spectrum of rubrene, with five bands centered at 2.22, 2.07, 1.92, 1.78, and 1.63 eV [Fig. 7(a)]. The intrinsic PL spectrum emitted by the ab facet of rubrene [Fig. 6(b)] can be accurately reproduced by a superposition of two progressions [Fig. 7(b)]. The first progression consists of four bands centered at 2.04, 1.90, 1.76, and 1.62 eV, separated by 0.140 eV. The second progression is identical to the one in Fig. 7(a), and corresponds to the one for c-polarized emission [dash-dotted lines in Fig. 7(b); the lower-energy bands are not shown because of their negligibly small amplitudes]. The reason behind the presence of a replica of the c-polarized progression in the ab-polarized PL spectrum is again the "leakage" of the c-polarized emission with its very large relative intensity. A detailed discussion of this and other artifacts affecting the experimental PL spectrum is given next.

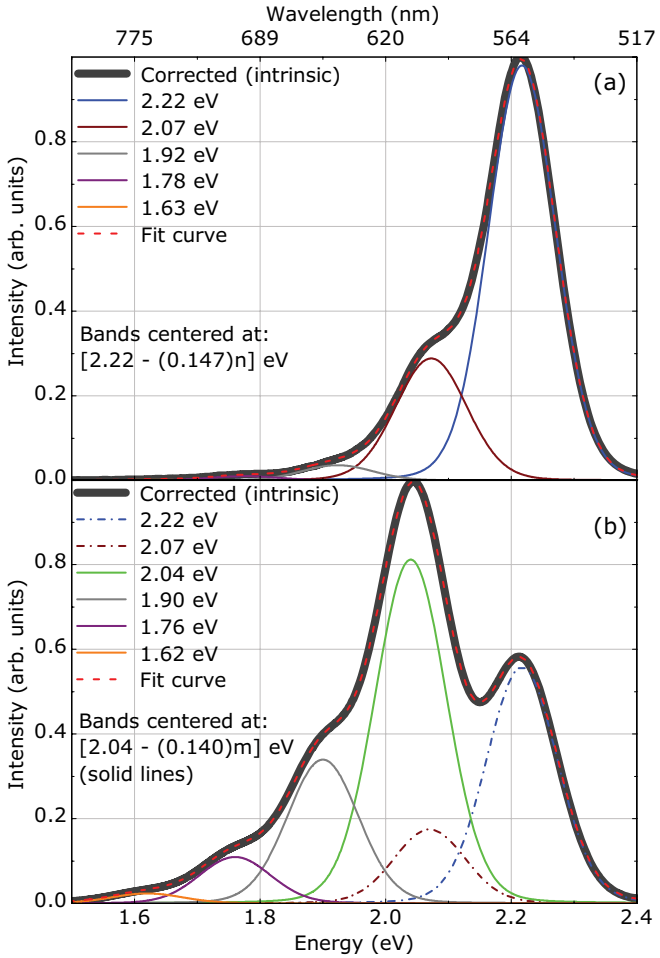

FIG. 7. (Color online) Peak fit of the corrected PL spectra from the bc (a) and ab (b) facets.

IV. DISCUSSION OF POSSIBLE EXPERIMENTAL ARTIFACTS

The most striking feature of the rubrene photoluminescence spectra is that the majority of the PL is emitted with c polarization. The peak of the c-polarized emission is 20 times larger in intensity than the peak of the a- or b-polarized PL that can be detected from an ab facet. This large anisotropy in PL matches the large absorption anisotropy observed in Fig. 3.

When determining the PL spectrum of a rubrene crystal, the strong c-polarized emission can cause a number of experimental artifacts. This is particularly true when measuring as-grown rubrene crystals with large ab facets. Since most rubrene crystals are flat platelets with the surface perpendicular to the c axis, upon excitation there will always be a very strong c-polarized emission that propagates away from the excitation point in all directions parallel to the ab surface. When capturing PL light into a small solid angle in a direction perpendicular to the ab surface of the crystal, the amount of c-polarized light that is detected can be quite small. It will increase if the solid angle increases (detection from a closer distance, or with shorter focal length lens in a confocal geometry) or for small deviations from the perpendicular direction. In addition to this, the less absorbed spectral component (the long-wavelength part) of the PL light propagating from the excitation point inside the flat crystal will be the one reaching the edges of the crystal. Detection of any light scattered from the edges of the crystal would then cause an artificial enhancement of the longer-wavelength portion of the spectrum. Finally, micrometer-sized mechanical imperfections that are often present on the crystal surface can cause scattering of the c-polarized light present inside the crystal, and this effect will redirect the c-polarized light into the detection system. Thus, scattering by surface imperfections can give rise to the appearance of a strong PL band centered around 2.22 eV even in configurations where the detection system is nominally set up to detect a- or b-polarized light.

Figure 8 gives examples of spectra affected by all these artifacts, from the variations of the detected PL spectrum with numerical aperture of the detection system [Fig. 8(a)], to the variations when tilting the crystal [Fig. 8(b)], to the effect of scattering centers on the surface [Fig. 8(c)], and finally to the strong redshift of the spectra observed when detecting the light that has propagated a long way in a rubrene platelet [Fig. 8(d)].

The effect of imperfections at the crystal surface is particularly important when measuring PL spectra using a collimated laser beam with a relatively large cross section.

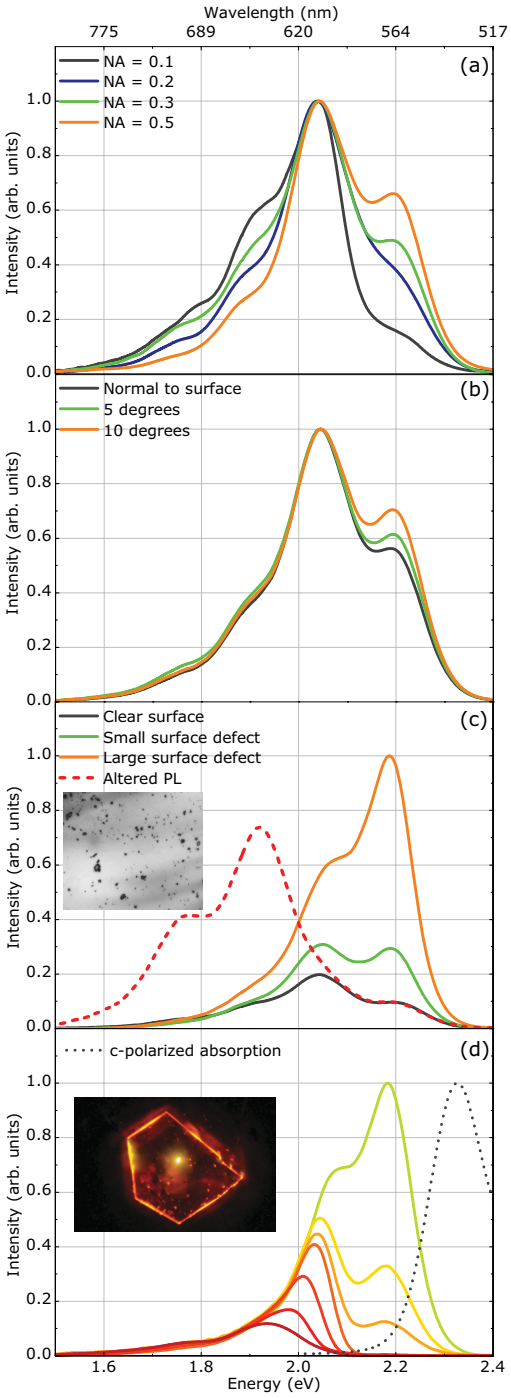

FIG. 8. (Color online) (a) PL spectra collected from *ab* facet with various numerical apertures. (b) PL spectra observed at various angles from the normal to the *ab* facet. (c) modification of the observed PL spectrum due to surface defects in the excitation/detection region. Inset: image of a surface of a rubrene crystal covering 90×60 micrometers. The dashed red curve shows the strongly altered PL spectrum that can sometimes be found in rubrene samples and is discussed in the text. (d) Effect of reabsorption on the PL spectrum emitted from the edge of a crystal with illumination at various distances from the edge. Inset: waveguiding of light in thin platelets of rubrene. The bright spot in the center corresponds to the focused excitation beam. All other crystal defects and the edges of the crystal glow because of scattering of the *c*-polarized light that propagates parallel to the *ab* surface.

Under such circumstances, several micrometer-sized defects can be present in the illuminated area, and they will scatter some *c*-polarized light, creating a larger shoulder around 2.22 eV in the PL spectrum. We experimentally confirmed under the microscope that this effect is very strong [Fig. 8(c)], with any defect in the excitation area appearing as a bright source of yellow (2.22 eV) light on top of a dimmer orange (2.04 eV) photoluminescence. This effect explains the strong variability of the PL spectra obtained from different regions on the surface of the same rubrene crystal. But we want to stress that, with a good control over surface quality under the microscope, we observed a perfect reproducibility of the rubrene PL spectrum obtained from tens of crystals of various shapes and sizes. PL measurements from facets other than the naturally extended *ab* facet ($\{001\}$ surface) are not as sensitive to surface quality, but unfortunately, most PL studies reported to date in rubrene relied on PL collection from the *ab* facet, which is usually the largest one in as-grown crystals.

The dominance of the *c*-polarized PL emission and the effect of scattering centers on the surface can also be directly visualized thanks to the strong self-guiding of light in thin platelet-like crystals with extended *ab* surfaces [Fig. 8(d), inset]. The majority of the radiated *c*-polarized PL lies within the critical angle for total internal reflection. As can be seen on the inset of Fig. 8(d), it is guided from the excitation spot towards the edges, and is then scattered both at the edges and on its way to the edges by surface imperfections and cracks. At the same time, there is a strong reabsorption while the *c*-polarized light propagates away from the excitation spot, and only the longer-wavelength portions of the emission reach the edges of the crystal. We demonstrated this effect by illuminating the *bc* facet of an elongated rubrene crystal at various distances from the edge (between 1 μm and 1 mm), while collecting the photoluminescence from the edge with a fiber. The evolution of the detected PL spectrum with increasing distance between the edge and the excitation spot is shown in Fig. 8(d) together with the normalized *c*-polarized absorption spectrum of rubrene.

We have shown that the high-energy shoulder at 2.22 eV in the PL emission spectrum of rubrene obtained from *ab* facets is an artifact created by the leakage of the strong *c*-polarized luminescence typical of rubrene. It can be minimized by ensuring a good crystal surface quality, precise crystal alignment, and by reducing the numerical aperture of the PL detection. The dark grey curve in Fig. 8(a) is an example of almost perfect PL measurement from the *ab* facet. The presence of the "leaking" *c*-polarized progression is minimized here, which produces a slight relative enhancement of lower-energy *b*-polarized bands, because the spectra were normalized to their peak. A complete removal of this artifact is practically impossible, given the nature of the radiation pattern of the *c*-polarized dipole and its relative strength.

To summarize, highly anisotropic absorption and emission of rubrene single crystals, a strong reabsorption of the PL spectrum due to an overlap between PL and absorption curves, and a high sensitivity to the surface quality account for a large variability of the reported PL spectra in the literature. If the effects described above are not taken into account, the resulting spectra can be mistakenly measured as redshifted (reabsorption) and position dependent (mechanical imperfections on surface). For example, in Ref. 16 a stronger

high-frequency band in the PL spectrum was observed in the presence of pyramidal structures on the *ab* surface of rubrene. This observation was interpreted as exciton confinement, while we show here that it must instead be related to scattering of *c*-polarized emission by the pyramidal structures on the surface. Reference 13 compared PL spectra of rubrene solutions at different concentrations with rubrene powder and crystals. The observed shift in the PL peak position was attributed to an increased intermolecular interaction, while in reality it is mostly caused by reabsorption. Reference 21 observed modifications in PL spectra of different polymorphs of rubrene microcrystals and proposed that "the remarkable difference in PL spectra might reflect a substantial change of exciton activities during relaxation." However, spectra obtained from different polymorphs of rubrene are expected to be affected by reabsorption to a different degree, and must be corrected for this artifact before a direct comparison can be made. Reference 15 attributed a 60 nm shift of the crystal PL peak relative to solution to strong intermolecular interactions in crystalline rubrene, and Ref. 17 explained similar spectral variations as "the emission presumably occurs from significantly red-shifted states, e.g., luminescent traps." However, the observed variations can instead be assigned to the fact that the crystal PL spectrum was likely collected from the *ab* facet, and cannot be directly compared to the PL emission of rubrene in a solution, as discussed above.

Furthermore, PL spectra obtained in systems other than macroscopic single crystals are affected by the same experimental artifacts described above. Reference 31,32 present PL spectra of rubrene nanoparticles, while Ref. 33 discusses PL emission originating from rubrene nanowire arrays. While all presented spectra show visible variations, such variations are likely to originate from the same unique intrinsic spectrum, modified by circumstances of excitation/detection. Of course, precise modeling of reabsorption in the absence of perfect crystalline arrangement is complicated, especially given a lack of information on how the spectra were obtained. Still, we believe that the large observed variations in the published rubrene PL spectra are mostly caused by variations in the excitation/detection geometry, and are not directly caused by size effects or morphology. From the point of view of PL spectroscopy, rubrene single crystals behave like an oriented molecular gas of isolated rubrene molecules, which is consistent with the expected weak intermolecular interaction forces in molecular crystals. As we have shown, the optical spectra of a molecule in solution and of a single crystal are very similar [Fig. 2(c)], with the crystal spectrum retaining all main spectral features of individual molecules.

After having identified the most prominent high-energy bands in the PL emission spectrum of rubrene and how they can be affected by the experimental configuration of excitation and detection, we now discuss the lower-energy PL bands. These bands can be seen in all the PL spectra that we reported above, near 1.92 and 1.78 eV, and are likely to be vibronic replicas of higher-energy bands. At the same time, enhanced PL bands at the same energies were reported and attributed to defect-related states that could originate from surface oxidation (see, for example, Refs. 18,20, and 34). The precise origin and the reason behind the observed modifications of the rubrene PL spectrum at long wavelengths is still being debated, and some recent reports exclude oxygen as a reason for the 1.9 eV band enhancement.[35] We observe that the amplitude of the band at around 1.78 eV *slightly* saturates at higher excitation intensities [Figs. 9(a) and 9(b)] and at higher temperatures [Figs. 9(c) and 9(d), accompanied by noticeable band broadening and overall PL intensity quenching]. However, prolonged exposure

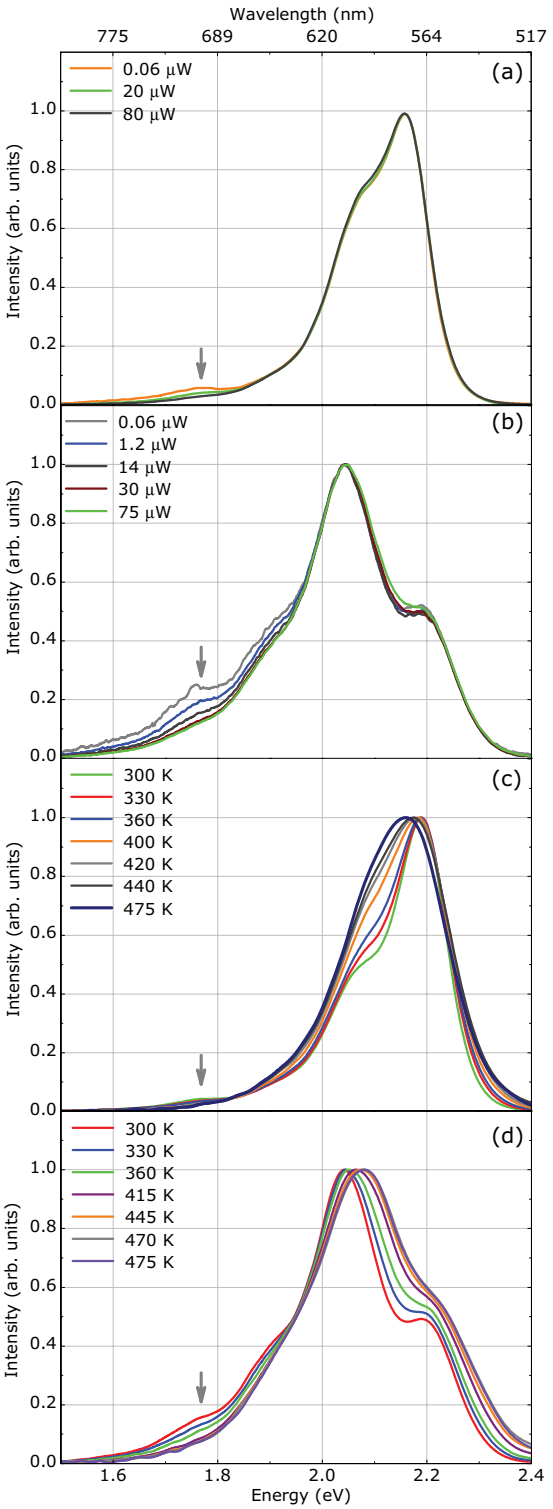

FIG. 9. (Color online) Normalized PL spectra collected from the *bc* (a) and *ab* (b) facets at various excitation powers. Normalized PL spectra collected from *bc* (c) and *ab* (d) facets at various temperatures.

to white light or laser emission in air did not result in any changes in the PL spectrum of high-quality stubby single crystals (see the Introduction), and we observed a remarkable stability and reproducibility in the relative amplitudes of PL bands in tens of single crystals like those shown in Fig. 1(d).

Some of the *thin crystalline films* of rubrene kept unprotected for a long time can develop a strongly altered PL spectrum, with strong low-energy bands dominating the spectrum, like the spectra reported in Refs. 13,14,22, and 35. An example of such a strongly altered spectrum is shown in Fig. 8(c). We observed this altered PL emission to have a strong saturation behavior at higher excitation powers, which may be caused by a strong temperature dependence connected with laser heating. The amplitudes of the lower-energy bands in this altered spectrum can also vary depending on the region of the crystal investigated, and the degree of alteration, but Fig. 8(b) shows a particularly clear example. The precise nature of this altered PL spectrum that peaks near 1.9 eV is not clear. In Ref. 22 a large difference between such a strongly altered PL spectrum of a rubrene single crystal and that of rubrene in solution was attributed to either oxidation or a presence of amorphous inclusions in the crystal, following Ref. 35. However, we have measured this altered spectrum to be *strongly polarized*, which indicates that its source remains *crystalline*. This would be consistent with Ref. 36 which demonstrated the formation of a crystalline rubrene peroxide layer above pristine rubrene crystalline domains. Sometimes two phases (with normal and altered spectrum) can coexist inside the same sample, with sharp boundaries between domains that are sometimes visible under an optical microscope, which is also consistent with the observations in Ref. 36. Regions with this altered spectrum have a noticeably higher PL quantum yield at lower excitation powers. It must be noted that the PL bands that dominate this altered spectrum are near the possible vibronic replicas of the *c*-polarized PL spectrum of pristine rubrene that we have identified close to 1.78 and 1.92 eV [see Fig. 7(a)]. We observed that a solution prepared from a rubrene sample with altered PL possesses absorbance and PL spectra identical to that of pristine rubrene. Reference 37 showed an appearance of a large peak in the density of trap states at 0.27 eV above the valence band after exposure of rubrene single crystals to oxygen and light, which would be energetically consistent with this strongly altered PL spectrum. On the other hand, Refs. 38 and 39 argue that the HOMO of oxidized rubrene has an energy $\sim$1 eV lower than that of rubrene, and cannot account for the band gap acceptor state, and propose instead that the presence of oxidized molecules disturbs the long-range periodicity and the delocalized nature of the HOMO in the crystal, also acting like point defects that produce localized acceptor states and can reduce carrier mobility. This would agree well with our own observation of a reduction of exciton diffusion length (see Ref. 30 for the method used to determine the diffusion length and for pristine rubrene data) in rubrene samples with altered PL spectrum, but for the moment the available data does not allow any definitive conclusions.

To conclude this section dedicated to experimental artifacts, we repeat that typical distortions of the PL spectrum that have been reported in the literature are the appearance of an abnormally strong band close to 2.2 eV when measuring normal to the *ab* surface, and a redshift of the peak of the PL spectrum caused by reabsorption. In addition, in some rubrene samples one sometimes finds regions that display a strongly altered PL spectrum that peaks around 1.9 eV, but is not caused by reabsorption effects. The material modifications that give rise to this strongly altered spectrum are at present still an open question. Special care needs to be taken when selecting rubrene single crystals for experiments intended to reveal intrinsic properties of pristine rubrene. In particular, the unclear origin of the strongly altered PL spectrum peaking near 1.9 eV, observed in Refs. 13,14,22, and 35, and shown with a dashed line in Fig. 8(c), casts doubts on the interpretation of measurements, like those in Ref. 22, that have been performed on crystals characterized by this altered PL spectrum that does not correspond to pristine orthorhombic rubrene.

V. DISCUSSION

Figure 10 shows a summary of the intrinsic absorption and emission spectra of rubrene. Figure 10(a) reproduces the *c*-polarized absorption and emission spectrum from Figs. 3(c) and 7(a). Figure 10(b) shows the *ab*-polarized absorption and emission spectrum of rubrene, as it can be obtained from the experimental spectrum of Figs. 3(a), 3(b), and 7(b) when eliminating the spectral components at 2.32

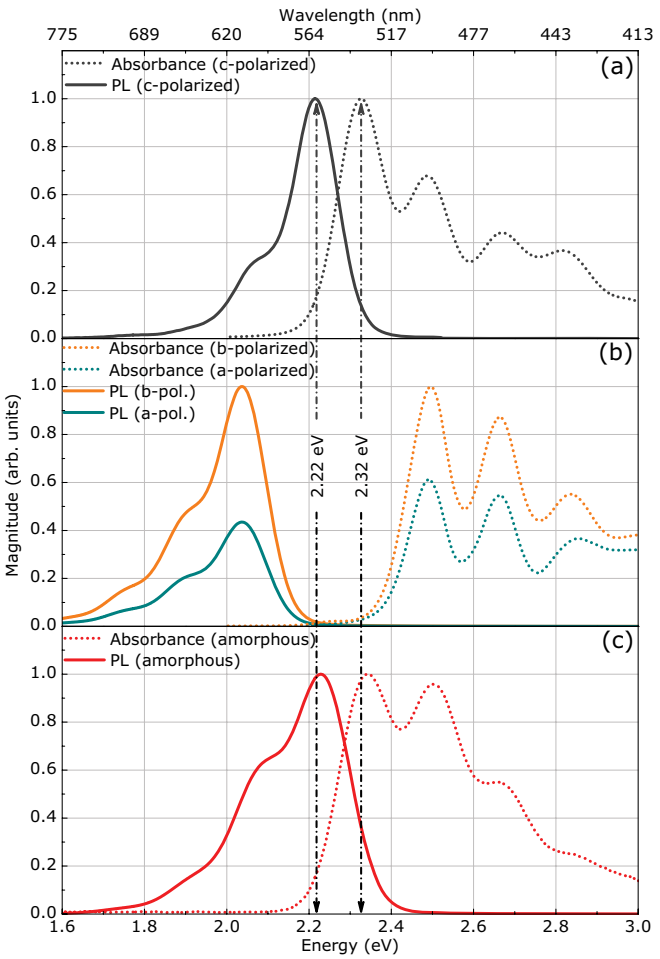

FIG. 10. (Color online) Intrinsic absorbance and PL spectra of rubrene.

eV (absorption) and 2.22 eV (emission) that we have assigned to leakage of the c-polarized spectrum. Figure 10(c) shows the absorption/emission of amorphous rubrene, which we obtained by melting rubrene in an enclosure protected from atmospheric influences.

To understand the final intrinsic absorption and emission spectra presented in Fig. 10, we first recall the expectations for the rubrene molecule as found in the rubrene crystal, which has a C_{2h} symmetry with a twofold rotational symmetry along the M axis and a mirror plane perpendicular to it.[23]

Quantum chemistry computations predict that the first optical absorption corresponding to the lowest-energy HOMO-LUMO transition in the rubrene molecule occurs around 2.3 eV, coupling only to light linearly polarized along the M axis.[28] The next higher electronic transition is predicted to be around 0.3–0.55 eV higher in energy, to be much weaker, and to couple to light linearly polarized perpendicular to the M-axis. The first HOMO-LUMO transition in the rubrene molecule, which is M-polarized, directly maps to c-polarized absorption in the rubrene crystal, where all molecules have their M axis exactly parallel to the c direction.[23] In fact, the c-polarized absorption spectrum as seen in Fig. 10(a) has a strong lowest-energy absorption peak at 2.32 eV, and so does the spectrum of amorphous rubrene, where the M axis will again dominate the optical properties. This first absorption peak at 2.32 eV can be assigned to a transition from the lowest vibrational state of the ground state to the lowest vibrational state of the first electronic excited state, while the higher-energy peaks can be assigned to excitation to higher vibrational levels, building a vibronic progression. This is consistent with the fact that no other c-polarized absorption is expected below 3 eV. The c-polarized PL spectrum also agrees with this picture, with a highest-energy emission peak at 2.22 eV, that can be understood as a transition from lowest vibrational state of the excited state to the lowest vibrational state of the ground state, followed by a rapidly decaying vibronic progression that corresponds to transitions to higher vibrational levels of the ground state.

The c-polarized absorption-emission spectrum of rubrene is qualitatively similar to that of other aromatic crystals such as tetracene. The larger Stokes shift of 0.10 eV in rubrene when compared to tetracene can be assigned to the larger number of lower frequency vibrational modes of the rubrene molecule.[25] The distances in the vibronic progressions (0.17 eV in absorption, 0.15 eV in emission) correspond to the frequency of vibrational modes involving the stretching of carbon-carbon bonds.[25,40] From the point of view of carbon-carbon stretching vibrations, the absorption/emission transitions at 2.32/2.22 eV can be considered "zero-phonon" transitions. In addition to the peaks of the vibronic progression, we have noted before that the c-polarized absorption spectrum has an observable additional absorption located at around 2.8 eV and with a width of about 0.25 eV (FWHM). This matches to the quasiparticle absorption edge as predicted by Sai *et al.*[28] A similar enhancement in the c-polarized absorption around 2.8 eV has also been seen by Tavazzi *et al.*[29]

The a- or b-polarized absorption of rubrene is much weaker (by factors of 7 and 4 peak to peak) than the c-polarized absorption. The spectra for both polarizations are very similar to each other and, once corrected for possible admixture of c-polarized absorption caused by experimental factors, are characterized by a first strong absorption peak at 2.49 eV, followed by a vibronic progression of decreasing strength until the spectrum starts being strongly influenced by the low-energy tail of the second electronic excited state with peak absorption near 3.7 eV (which couples to LN polarized radiation in the molecule reference frame and hence to ab-polarized radiation in the crystal reference frame). The ab-polarized emission spectrum is a reflection of the corresponding absorption spectrum. Here, too, a small band close to 2.22 eV is most likely caused by an experimentally difficult-to-control leakage of c-polarized emission. In this view, the highest energy emission peak is observed at 2.04 eV, followed by a vibronic progression separated by 0.14 eV.

The ab-polarized absorption and emission as seen in Fig. 10 cannot be assigned to a transition between ground state and an electronic excited state that has a transition dipole moment with components along the a or b axis of the crystal (LN axes of the molecule). First of all, the predicted oscillator strength for the second available electronic excited state in rubrene with an LN transition dipole moment is very weak.[28] Secondly, the excitation energy predicted for this transition is clearly larger than the observed first ab-polarized absorption peak at 2.49 eV. We have recalculated the electronic transitions of the rubrene molecule using Time-dependent density functional theory (TDDFT) at the B3LYP/6-31G level of theory as well as using the Zerner's Intermediate Neglect of Differential Overlap (ZINDO) method[41,42] as implemented in GAUSSIAN 03,[43] and no dipole-allowed transition beyond HOMO-LUMO is predicted at energies matching the onset of the ab-polarized absorption. It should also be noted that the ab-polarized absorption peaks and their vibronic progressions accurately match the higher vibrational peaks in the c-polarized spectrum. It would be difficult to discount this as a coincidence. We therefore conclude, contradicting the hypothesis of Tavazzi *et al.*,[14] but consistently with the calculations of Sai *et al.*,[28] that the first ab-polarized absorption peak cannot be assigned to a second electronic transition in the rubrene molecule.

We argue that the ab-polarized absorption and emission in the rubrene single crystal can be due to a depolarization induced by molecular vibrations of the first M-oriented excitation. This vibronically induced depolarization of the HOMO-LUMO transition can be understood as the interaction of the $A_g \leftrightarrow A_u$ electronic excitation with a vibrational mode, with appropriate symmetry, of the ground state (for emission) or of the excited state (for absorption). Similarly to the previous discussion of electronic states, the C_{2h} symmetry of the molecules in the rubrene crystal allows vibrational modes with four symmetry types: a_g, a_u, b_g, and b_u (we use lower-case letters to distinguish from the symmetry of electronic states, represented by capital letters). Starting from the vibrationless $A_g \rightarrow A_u$ transition of the molecule, which is entirely c polarized in a crystal with rigid molecules, one can see that a dipole excitation to the A_u state that is in some b_g vibrational mode would be LN polarized. Recalling that the (L,N,M) components of the dipole operator in the C_{2h} point group transform as (B_u,B_u,A_u), it is easy to see that the dipole operator components along L or N, which have B_u symmetry, can create a transition between the A_g ground state and an excited state vibrational mode that has symmetry b_g:

$A_g \otimes B_u \otimes (A_u \otimes b_g) = A_g$. On the other hand, excitations to some a_g vibrational mode of the excited state can be induced by a dipole operator component along M, which has symmetry A_u: $A_g \otimes A_u \otimes (A_u \otimes a_g) = A_g$. An analogous argument can be made for PL transitions. It follows that the ab-polarized vibrational progression in the crystal's absorption-emission spectra can be caused by transitions to higher vibrational modes that have symmetry b_g, while the vibronic progression in the c-polarized absorption-emission spectra can be caused by transitions to higher vibrational states with a_g symmetry. If the a_g and b_g modes have similar frequencies, then the c-polarized and the ab-polarized peaks would have almost the same position in the spectra, but the vibrationless transition would only be observed in the c-polarized spectrum. This is exactly what is seen in the absorption spectra of Fig. 10. The vibrationless HOMO-LUMO transition is only observed in the c-polarized spectra, while as soon as a transition is to a higher vibrational state, then it can couple to ab-polarized light.

The totally symmetric vibrational mode of the excited state responsible for the vibrational progression in absorption is likely the one calculated at 1331 cm^{-1} (0.165 eV) in Ref. 25, which has the largest normal coordinate displacement. Ground-state vibrational modes with appropriate symmetry, which could be responsible for the vibrational progressions observed in the PL spectra, have been seen in the Raman measurements of Ref. 40 near 1163 cm^{-1} (0.144 eV).

In conclusion, we have determined the intrinsic anisotropic polarized absorption and emission spectra of orthorhombic rubrene. We described the effects of reabsorption on observed photoluminescence spectra, and discussed the experimental pitfalls that can produce deformed PL spectra measured in crystals with imperfect surfaces or in general when the strong c-polarized emission is not controlled when obtaining spectra that nominally belong to a- or b-polarized light. Finally, we reviewed the possible electronic and vibronic transitions in rubrene and assigned the a- or b-polarized absorption and emission in the visible and near infrared spectral range to vibronically induced depolarization of the electronic HOMO-LUMO transition.

ACKNOWLEDGMENTS

We thank V. Podzorov at Rutgers University for providing us with rubrene crystals.

[1] V. C. Sundar, J. Zaumseil, V. Podzorov, E. Menard, R. L. Willett, T. Someya, M. E. Gershenson, and J. A. Rogers, Science **303**, 1644 (2004).
[2] A. Briseno, R. Tseng, M.-M. Ling, E. Falcao, Y. Yang, F. Wudl, and Z. Bao, Adv. Mater. **18**, 2320 (2006).
[3] R. de Boer, M. Gershenson, A. Morpurgo, and V. Podzorov, Phys. Status Solidi A **201**, 1302 (2004).
[4] R. Tseng, R. Chan, V. Tung, and Y. Yang, Adv. Mater. **20**, 435 (2008).
[5] Y. Shao and Y. Yang, Appl. Phys. Lett. **86**, 073510 (2005).
[6] V. Podzorov, V. Pudalov, and M. Gershenson, Appl. Phys. Lett. **82**, 1739 (2003).
[7] V. Podzorov, E. Menard, A. Borissov, V. Kiryukhin, J. A. Rogers, and M. E. Gershenson, Phys. Rev. Lett. **93**, 086602 (2004).
[8] V. Podzorov and M. E. Gershenson, Phys. Rev. Lett. **95**, 016602 (2005).
[9] T. Hasegawa and J. Takeya, Sci. Technol. Adv. Mate. **10**, 024314 (2009).
[10] H. Najafov, I. Biaggio, V. Podzorov, M. F. Calhoun, and M. E. Gershenson, Phys. Rev. Lett. **96**, 056604 (2006).
[11] H. Najafov, B. Lyu, I. Biaggio, and V. Podzorov, Phys. Rev. B **77**, 125202 (2008).
[12] H. Najafov, B. Lyu, I. Biaggio, and V. Podzorov, Applied Phys. Lett. **96**, 183302 (2010).
[13] X. Zeng, D. Zhang, L. Duan, L. Wang, G. Dong, and Y. Qiu, Appl. Surf. Sci. **253**, 6047 (2007).
[14] S. Tavazzi, A. Borghesi, A. Papagni, P. Spearman, L. Silvestri, A. Yassar, A. Camposeo, M. Polo, and D. Pisignano, Phys. Rev. B **75**, 245416 (2007).
[15] A. Saeki, S. Seki, T. Takenobu, Y. Iwasa, and S. Tagawa, Adv. Mater. **20**, 920 (2008).
[16] R. J. Stohr, G. J. Beirne, P. Michler, R. Scholz, J. Wrachtrup, and J. Pflaum, Appl. Phys. Lett. **96**, 231902 (2010).
[17] M. Müller, A. Langner, O. Krylova, E. Le Moal, and M. Sokolowski, Appl. Phys. B **105**, 67 (2011).
[18] O. Mitrofanov, C. Kloc, T. Siegrist, D. V. Lang, W.-Y. So, and A. P. Ramirez, Appl. Phys. Lett. **91**, 212106 (2007).
[19] H. Liu, F. Yan, W. Li, C.-S. Lee, B. Chu, Y. Chen, X. Li, L. Han, Z. Su, J. Zhu, X. Kong, L. Zhang, and Y. Luo, Org. Electron. **11**, 946 (2010).
[20] C. Kloc, K. J. Tan, M. L. Toh, K. K. Zhang, and Y. P. Xu, Appl. Phys. A. **95**, 219 (2009).
[21] L. Huang, Q. Liao, Q. Shi, H. Fu, J. Ma, and J. Yao, J. Mater. Chem. **20**, 159 (2010).
[22] L. Ma, K. Zhang, C. Kloc, H. Sun, M. E. Michel-Beyerle, and G. G. Gurzadyan, Phys. Chem. Chem. Phys. **14**, 8307 (2012).
[23] O. D. Jurchescu, A. Meetsma, and T. T. M. Palstra, Acta Crystallogr. Sect. B **62**, 330 (2006).
[24] D. Käfer, L. Ruppel, G. Witte, and C. Wöll, Phys. Rev. Lett. **95**, 166602 (2005).
[25] T. Petrenko, O. Krylova, F. Neese, and M. Sokolowski, New J. Phys. **11**, 015001 (2009).
[26] M. El Helou, O. Medenbach, and G. Witte, Crystal Growth Design **10**, 3496 (2010).
[27] W. Kaminsky, J. Appl. Crystallogr. **38**, 566 (2005).
[28] N. Sai, M. L. Tiago, J. R. Chelikowsky, and F. A. Reboredo, Phys. Rev. B **77**, 161306 (2008).
[29] S. Tavazzi, L. Silvestri, M. Campione, A. Borghesi, A. Papagni, P. Spearman, A. Yassar, A. Camposeo, and D. Pisignano, J. Appl. Phys. **102**, 023107 (2007).
[30] P. Irkhin and I. Biaggio, Phys. Rev. Lett. **107**, 017402 (2011).
[31] S. Köstler, A. Rudorfer, A. Haase, V. Satzinger, G. Jakopic, and V. Ribitsch, Adv. Mater. **21**, 2505 (2009).
[32] D. H. Park, S. G. Jo, Y. K. Hong, C. Cui, H. Lee, D. J. Ahn, J. Kim, and J. Joo, J. Mater. Chem. **21**, 8002 (2011).

[33]J. W. Lee, K. Kim, D. H. Park, M. Y. Cho, Y. B. Lee, J. S. Jung, D.-C. Kim, J. Kim, and J. Joo, Adv. Funct. Mater. **19**, 704 (2009).

[34]O. Mitrofanov, D. V. Lang, C. Kloc, J. M. Wikberg, T. Siegrist, W.-Y. So, M. A. Sergent, and A. P. Ramirez, Phys. Rev. Lett. **97**, 166601 (2006).

[35]Y. Chen, B. Lee, D. Fu, and V. Podzorov, Adv. Mater. **23**, 5370 (2011).

[36]E. Fumagalli, L. Raimondo, L. Silvestri, M. Moret, A. Sassella, and M. Campione, Chem. Mater. **23**, 3246 (2011), http://pubs.acs.org/doi/pdf/10.1021/cm201230j.

[37]C. Krellner, S. Haas, C. Goldmann, K. P. Pernstich, D. J. Gundlach, and B. Batlogg, Phys. Rev. B **75**, 245115 (2007).

[38]Y. Nakayama, S. Machida, T. Minari, K. Tsukagishi, Y. Noguchi, and H. Ishii, Appl. Phys. Lett. **93**, 173305 (2008).

[39]X. Song, L. Wang, Q. Fan, Y. Wu, H. Wang, C. Liu, N. Liu, J. Zhu, D. Qi, X. Gao, and A. T. S. Wee, Appl. Phys. Lett. **97**, 032106 (2010).

[40]J. R. Weinberg-Wolf, L. E. McNeil, S. Liu, and C. Kloc, J. Phys.: Condens. Matter **19**, 276204 (2007).

[41]J. Ridley and M. Zerner, Theor. Chim. Acta **32**, 111 (1973).

[42]M. C. Zerner, G. H. Loew, R. F. Kirchner, and U. T. Mueller-Westerhoff, J. Am. Chem. Soc. **102**, 589 (1980), http://pubs.acs.org/doi/pdf/10.1021/ja00522a025.

[43]M. J. Frisch, G. W. Trucks, H. B. Schlegel, G. E. Scuseria, M. A. Robb, J. R. Cheeseman, J. A. Montgomery, Jr. T. Vreven, K. N. Kudin, J. C. Burant, J. M. Millam, S. S. Iyengar, J. Tomasi, V. Barone, B. Mennucci, M. Cossi, G. Scalmani, N. Rega, G. A. Petersson, H. Nakatsuji, M. Hada, M. Ehara, K. Toyota, R. Fukuda, J. Hasegawa, M. Ishida, T. Nakajima, Y. Honda, O. Kitao, H. Nakai, M. Klene, X. Li, J. E. Knox, H. P. Hratchian, J. B. Cross, V. Bakken, C. Adamo, J. Jaramillo, R. Gomperts, R. E. Stratmann, O. Yazyev, A. J. Austin, R. Cammi, C. Pomelli, J. W. Ochterski, P. Y. Ayala, K. Morokuma, G. A. Voth, P. Salvador, J. J. Dannenberg, V. G. Zakrzewski, S. Dapprich, A. D. Daniels, M. C. Strain, O. Farkas, D. K. Malick, A. D. Rabuck, K. Raghavachari, J. B. Foresman, J. V. Ortiz, Q. Cui, A. G. Baboul, S. Clifford, J. Cioslowski, B. B. Stefanov, G. Liu, A. Liashenko, P. Piskorz, I. Komaromi, R. L. Martin, D. J. Fox, T. Keith, M. A. Al-Laham, C. Y. Peng, A. Nanayakkara, M. Challacombe, P. M. W. Gill, B. Johnson, W. Chen, M. W. Wong, C. Gonzalez, and J. A. Pople, "GAUSSIAN 03 Revision C.02", Gaussian, Inc., Wallingford CT, 2004.